Eur Biophys J (2008) 37:435–445
DOI 10.1007/s00249-007-0233-4

ORIGINAL PAPER

Secondary structure and distribution of fusogenic LV-peptides in lipid membranes

J. Ollesch · B. C. Poschner · J. Nikolaus · M. W. Hofmann · A. Herrmann · K. Gerwert · D. Langosch

Received: 6 August 2007 / Revised: 11 October 2007 / Accepted: 28 October 2007 / Published online: 24 November 2007

Abstract LV-peptides were designed as membrane-spanning low-complexity model structures that mimic fusion protein transmembrane domains. These peptides harbor a hydrophobic core sequence that consists of helix-promoting and helix-destabilizing residues at different ratios. Previously, the fusogenicity of these peptides has been shown to increase with the conformational flexibility of their hydrophobic cores as determined in isotropic solution. Here, we examined the secondary structure, orientation, and distribution of LV-peptides in membranes. Our results reveal that the peptides are homogeneously distributed within the membranes of giant unilamellar liposomes and capable of fusing them. Increasing the valine content of the core up to the level of the β-branched residue content of SNARE TMDs ($\sim$50%) enhances fusogenicity while maintaining a largely α-helical structure in liposomal membranes. A further increase in valine content or introduction of a glycine/proline pair favors β-sheet formation. In planar bilayers, the α-helices adopt oblique angles relative to the bilayer normal and the ratio of α-helix to β-sheet responds more sensitively to valine content. We propose that the fusogenic conformation of LV-peptides is likely to correspond to a membrane-spanning α-helix. β-Sheet formation in membranes may be considered a side-reaction whose extent reflects conformational flexibility of the core.

J. Ollesch · K. Gerwert
Lehrstuhl für Biophysik, Ruhr-Universität Bochum,
Universitätsstr. 150, 44780 Bochum, Germany

Present Address:
J. Ollesch
Institute for Neurodegenerative Diseases,
University of California, San Francisco, 513 Parnassus Ave,
Box 0518, San Francisco, CA 94143-0518, USA

B. C. Poschner · M. W. Hofmann · D. Langosch (✉)
Lehrstuhl Chemie der Biopolymere,
Technische Universität München,
Freising and Munich Center for Integrated Protein Science,
CIPSM, Weihenstephaner Berg 3, 85354 Freising, Germany
e-mail: langosch@lrz.tum.de

J. Nikolaus · A. Herrmann
AG Molekulare Biophysik, Institut für Biologie,
Mathematisch-Naturwissenschaftliche Fakultät I,
Humboldt-Universität zu Berlin, Invalidenstr. 42,
10115 Berlin, Germany

Introduction

Fusion of lipid membranes is mediated by fusogenic integral membrane proteins. These include SNARE [soluble NSF(N-ethylmaleimide-sensitive factor) attachment protein receptor] proteins that drive intracellular fusion of eukaryotic membranes as well as a diverse group of proteins from enveloped viruses (Jahn and Scheller 2006; Langosch et al. 2007; Tamm et al. 2003). While soluble fusion protein domains are required to mediate close membrane apposition prior to actual fusion, there is ample evidence that their single transmembrane domains (TMDs) contribute to fusion at different stages of lipid mixing. For example, the fusion reaction is blocked at hemifusion upon replacing viral fusion protein TMDs by glycosylphosphatidylinositol (GPI) anchors or after mutating them (Armstrong et al. 2000; Cleverley and Lenard 1998; Kemble et al. 1994; Melikyan et al. 1999; Nüssler et al. 1997). Along the same line, truncating (Xu et al. 2005) or mutating (Hofmann et al. 2006) the TMDs of SNAREs, or replacing them by a GPI anchor (Giraudo et al. 2005)

partially arrested fusion at hemifusion. Hemifusion is defined by mixing of outer monolayers whereas inner monolayers stay separated. A proteinaceous TMD therefore supports inner leaflet mixing. The efficiency of inner leaflet mixing appears to depend also on TMD-TMD interactions since point mutations that weaken this interaction in the yeast SNARE Vam3p also decrease the efficiency of the hemifusion-to-fusion transition (Hofmann et al. 2006; Roy et al. 2006).

Transmembrane domains may also support outer leaflet mixing, i.e., initiation of fusion. This is suggested by the observation that wild-type influenza hemagglutinin (Armstrong et al. 2000) and SNAREs (Giraudo et al. 2005) were more efficient in driving outer leaflet mixing than the corresponding versions with GPI anchors in place of their TMDs (Langosch et al. 2007). That TMDs contribute to outer leaflet mixing is also indicated by the finding that synthetic peptides representing the TMDs of SNAREs (Hofmann et al. 2006; Langosch et al. 2001b) or of the Vesicular Stomatitis virus G-protein (Dennison et al. 2002; Langosch et al. 2001a) drive liposome–liposome fusion in vitro. Since these TMD-peptides are devoid of membrane-extrinsic domains that could mediate membrane apposition, it appears that isolated TMDs increase the likelihood by which randomly colliding liposomes enter fusion. Although the precise mechanism by which the TMD-peptides induce fusion is presently not clear, their activity has been related to conformational flexibility of the peptide backbone. Specifically, the TMD-peptides formed mixtures of α-helical and β-sheet structures in inverse micelles, and mutations that increased the abundance of the α-helical fraction decreased fusogenicity (Dennison et al. 2002; Langosch et al. 2001a, b). This is consistent with an unusual amino acid composition since the β-sheet promoting β-branched amino acids Val and Ile collectively make-up ~50% of SNARE TMD sequences but only ~25% of unrelated TMDs (Langosch et al. 2001b).

To test by de novo design whether TMD flexibility affects fusogenicity, low-complexity hydrophobic model sequences, termed LV-peptides, were developed. LV-peptides contain hydrophobic core sequences that are composed of residues with different secondary structure propensities, i.e., helix-promoting Leu and sheet-promoting Val residues at different ratios (Hofmann et al. 2004). Val is thought to destabilize helices due to loss of side-chain entropy upon helix formation (Chellgren and Creamer 2006). In some LV-peptides, the core sequences also contain a Gly/Pro or a Pro/Gly pair to further destabilize the helical conformation. Liposome–liposome fusion assays showed that a Leu-based peptide (L16) displays little fusogenicity while mixtures of Leu and Val exhibited intermediate (LLV16) to strong (LV16, VVL16) fusogenicity. Helix-destabilizing Gly/Pro (LV16-G8P9) or Pro/Gly (LV16-P8G9) pairs enhance fusion still further. In agreement with the α-helical structure of the TMDs from natural fusion proteins, like SNAREs (Bowen and Brunger 2006; Xu et al. 2005; Zhang and Shin 2006) or influenza hemagglutinin (Tatulian and Tamm 2000), LV-peptides form α-helices in trifluoroethanol (TFE). Consistent with the proposed relationship between fusogenicity and structural flexibility, only fusogenic peptides can readily be refolded from the α-helical conformation to β-sheet or vice versa by changing the ratio of TFE to aqueous buffer (Hofmann et al. 2004).

Here, we investigated the secondary structure and physical distribution of LV-peptides in membranes. Circular Dichroism (CD) and Attenuated Total Reflection Fourier Transform Infrared (ATR-FTIR) spectroscopy show that the membrane-associated peptides form mixed populations that fold into different secondary structures. The relative abundances of the secondary structure types depend on peptide sequence as does fusogenicity. It is proposed that the extent of β-sheet formation reflects the intrinsic flexibility of the α-helical state being an important determinant of fusion.

Experimental procedures

Peptide synthesis

Peptides were synthesized by Boc chemistry (PSL, Heidelberg, Germany) and were >90% pure as judged by mass spectrometry. Rhodamine-tagged peptides were made by coupling of a Lys derivative [Fmoc–Lys(Dde)–OH] to the C- and N-termini during synthesis. Reaction of the peptide with 5-(and-6)-carboxytetramethylrhodamine succinimidylester (TAMRA) yielded rhodamine-labeled peptides. Concentrations of unlabeled peptides were determined via tryptophan (Trp) absorbance using an extinction coefficient of 5,600 M^{-1} cm^{-1}.

Preparation of liposomes for CD spectroscopy

Liposomes were prepared by sonication as described (Langosch et al. 2001b) from mixtures of palmitoyl oleoyl phosphatidylcholine (POPC), di-oleoyl-phosphatidylethanolamine (DOPE), and di-oleoyl-phosphatidylserine (DOPS) (all from Avanti Polar Lipids) at a ratio of 3:1:1 (w/w/w). Prior to sonication the hydrated peptide/lipid mixture was subjected to 10 freeze/thaw cycles in liquid nitrogen. Peptide concentrations were determined by Trp fluorescence as described (Langosch et al. 2001a) except that liposomes were lyzed with 1% (w/v) SDS prior to the measurements.

Sucrose gradient centrifugation

The association of peptides with liposomes was examined upon separating unbound peptides from proteoliposomes by density gradient centrifugation (Langosch et al. 2001a). 300 µl of liposome preparations were mixed with 700 µl 60% (w/v) sucrose, and overlaid with 2.5 ml 30% (w/v) sucrose followed by 0.5 ml fusion buffer. Upon centrifugation (56,000 rpm, 20 h, 20°C, Beckman SW60 rotor, Fullerton, CA, USA), >99% of the loaded lipids were found in the top fraction. Peptides were found to quantitatively co-migrate with the lipid fraction, as Trp fluorescence was not detectable in the bottom fraction.

CD spectroscopy

CD spectra were measured with a Jasco J-810 automatic recording spectral polarimeter. Spectra of liposomes (1.5 mM lipid) were recorded from 200 to 240 nm in a 1-mm dichroically neutral quartz cuvette at 20°C by using a time constant of 4 s per scan speed of 100 nm min^{-1} and a sensitivity of 100 millidegrees per cm. Spectra represent the signal-averaged accumulation of ten scans. Baseline spectra were recorded with pure liposomes and subtracted from the spectra of peptide-containing liposomes. All spectra were converted to mean residue ellipticity (θ_{mr}), and secondary structures were calculated using the CDNN/PEPFIT algorithm that is based on a user-defined set of peptide-based reference spectra (Poschner et al. 2007).

FTIR spectroscopy

Thin stacks of oriented bilayers were prepared on an attenuated total reflection—internal reflection element (ATR-IRE) by lipid spreading and solvent evaporation as described (Seul and Sammon 1990). A mixture of synthetic DOPS, DOPE, and POPC at a 3:1:1 (w/w/w) ratio was used. About 100 µg Lipid, with 1 mol% peptide were spread from a solution of trifluoroethanol (TFE)/chloroform 1:1 on the 48 × 20 mm^2 and 52 × 20 mm^2 sides of a trapezoid germanium 25 internal reflection element (52 × 20 × 2 mm^3). After solvent evaporation, the sample films were vacuum-dried for at least 1 h.

Dry films were rehydrated in a stream of water-vapor-saturated nitrogen (~85% relative humidity). Extinction spectra were recorded after spectrum stability reached instrumental noise level. Experimental control by analysis of the dichroitic ratio of the lipid ester C = O vibration band at 1,735 cm^{-1} according to (Bechinger et al. 1999) yielded formation of five bilayers on average, as expected for the used amount of lipid. Samples were analyzed in a Bruker IFS66 FTIR spectrometer equipped with a vertical 25 internal reflection ATR setup (Specac) (45° incidence angle) and liquid nitrogen cooled MCT detector. About 256 interferograms were acquired for each single channel spectrum. Interferogram acquisition was double-sided with forward and backward mirror movement. Spectra were recorded with 2 cm^{-1} resolution and a factor four zero-filling, resulting in 1 datapoint each 0.32 cm^{-1}. Reference for an absorbance spectrum was the same blank internal reflection element (IRE) under identical conditions. Spectra were measured without and with KRS5 IR-polarizer set on 0° and 90° polarization toward the IRE surface. Bacteriorhodopsin (bR) control samples were analyzed with a Bruker IFS88 equipped with a 9 internal reflection µATR (SensIr, Smiths Detection, Smiths Group plc.) and a KRS-5 polarizer. About 2.5 µg Purple membrane suspension was adsorbed to the IRE surface by solvent evaporation. Unbound material was removed by rinsing with 2 ml H_2O. Spectra were measured as described before. Correction of water vapor, lipid, and bound liquid water contributions to the amide-I-region was carried out with spectra of water vapor as described (Goormaghtigh and Ruysschaert 1994) and of pure lipids identically prepared and hydrated, scaled with the lipid-ester vibration at ~1,735 cm^{-1}, accordingly. Spectra were smoothed by Fourier self-deconvolution as low-pass filter gating at 4 cm^{-1}. The conformation sensitive amide I band which represents backbone C = O stretching vibrations was decomposed into cauchy-curves for secondary structure quantification (Goormaghtigh et al. 1994). The relation of the component integrals to the overall amide I integral represented the secondary structure fraction assigned to its position. Identical initialization parameters for the numerical curve fitting procedure [band position, full width at half height (FWHH), band shape, number of bands and all parameter borders] for the whole series of spectra of one peptide increased the method's sensitivity for structural alterations (Ollesch et al. 2007). Initial component band intensities, overall baseline level, and tilt were automatically set for each amide I band. It was taken care to avoid overfitting and resulting parameters sticking to fitting boundaries. Bands were assigned to secondary structure depending on the position as commonly found in literature (Arrondo et al. 1993; Bandekar 1992; Byler and Susi 1986; Krimm and Bandekar 1986; Surewicz and Mantsch 1990; Surewicz et al. 1993). Orientational analysis of the α-helical peptide parts was performed using linear dichroism according to (Bechinger et al. 1999). We calculated the dichroitic ratio R from integrals of the α-helical components A_α determined with curve fits of spectra obtained with IR radiation polarized 0° or 90° to the IRE surface. The dichroitic ratio for systems of uniaxial symmetry (Harrick 1967) defines the system order parameter S via $R = A_\alpha(90°)/A_\alpha(0°) = E_x^2/E_y^2 + E_z^2/$

$E_y^2[1 + 3S/(1-S)]$, with the squared electric field intensities E_x^2, E_y^2, and E_z^2. Those are dependent on refractive indices of the IRE (4.0 for germanium), the lipid film (1.44) and the surrounding medium (nitrogen, 1.0), and were derived from thin film approximation (Goormaghtigh and Ruysschaert 1990). For the bR control, the sample refractive index had to be 1.7 to satisfy the high protein/lipid ratio of the purple membrane. The sample thickness demanded the use of the thick film approximation. The coordinate system was defined as a cartesian with x in plane of the IRE in direction of transmittance, y perpendicular in the IRE plane, and z perpendicular to both, thus perpendicular to the IRE surface.

S describes the observable order parameter of the system, which is interpreted as tilt of the sample of an angle θ from the IRE normal with $S = (3\cos^2\theta - 1)/2$.

The observed order parameter S can further be interpreted as a product of three system specific components S_α, S_β, and S_γ. These are S_α, describing the mean angle of deviation of the membrane normal to the IRE normal α, S_β, defining the mean angle of the peptide helix axis from the membrane normal β, and S_γ, which represents the mean angle of the dipole moment from the helix axis γ. Hence, the desired tilt angle β was calculated from $S_\beta = S/S_\alpha/S_\gamma$, and $\beta = [\arccos((2S_\beta + 1)/3)]^{1/2}$. S_α was estimated as 1 (Zhang et al. 1995) due to similar preparation conditions. While a range of angles up to 40° has been reported (Tatulian 2003), γ was previously determined to be 27° for bR (Rothschild 1979). This is a membrane protein. All of its α-helices span the lipid bilayer. Therefore, we considered $\gamma = 27°$ as appropriate approximation for our transmembrane peptides.

Preparation of giant unilamellar vesicles for confocal laser scanning microscopy

Giant unilamellar vesicles (GUVs) were prepared by the electroformation method (Angelova et al. 1992). In short, lipid mixtures of POPC, DOPE, and DOPS at a ratio of 3:1:1 (w/w/w) were made from stock solutions in chloroform. About 45 nmol of lipids were dissolved in 140 µl chloroform (final concentration of 0.25 mg ml^{-1}) along with 1 mol% of L-α-phosphatidylethanolamine-N-(lissamine rhodamine B sulfonyl) (N-Rh-PE) or 1,2-dipalmitoyl-*sn*-glycero-3-phosphoethanolamine-N-(7-nitro-2-1,3-benzoxadiazol-4-yl) (N-NBD-PE) or 1-palmitoyl-2-[6-[(7-nitro-2-1,3-benzoxadiazol-4-yl)amino]hexanoyl]-*sn*-glycero-3-phosphocholine (C6-NBD-PC) (all from Avanti Polar Lipids) and/or 1 mol% of Rh-LLV16 and Rh-LV16-GP, respectively, both dissolved in trifluoroethanol. This lipid/peptide solution was spotted in little droplets onto two ITO slides, which were heated during the procedure on a heating plate at about 50°C to facilitate solvent evaporation and to achieve a homogeneous distribution of the lipid film. ITO slides were exposed to high vacuum for 1.5 h for complete evaporation of the solvent. Lipid-coated slides were assembled with a 1 mm Teflon spacer. The chamber was filled with ~1 ml swelling buffer (250 mM sucrose, 15 mM NaN_3) with an osmolarity of 280 mOsm kg^{-1} and sealed with plasticine. An alternating electrical field rising from 0.02 to 1.1 V in the first 30 min with a frequency of 10 Hz was applied overnight at room temperature followed by 0.5 h of 4 Hz and 1.3 V to detach the formed liposomes. GUVs were stored at room temperature, shielded from light and used within the next days. To investigate lateral distribution of the peptides, suspensions of GUVs containing peptide and C6-NBD-PC were added to glucose buffer (250 mM glucose, 11.6 mM potassium phosphate, pH 7.2) with an osmolarity of 300 mOsm kg^{-1} at a ratio of 1:1–1:3. Prior to microscopy, GUVs were given some minutes to settle down on a coverslip. Confocal images of the equatorial plane of the GUV were taken with an inverted confocal laser scanning microscope (FV1000, Olympus, Tokyo, Japan) with a 60× (N.A. 1.35) oil-immersion objective at room temperature. The red rhodamine-fluorescence and the green NBD-fluorescence were excited with the 543 nm laser line of a HeNe laser (Melles Girot) and the 488 nm laser line of an Ar-ion laser (Melles Girot), respectively. The emissions of rhodamine and NBD were recorded between 569 and 669 nm and between 500 and 510 nm, respectively.

To investigate GUV-GUV fusion mediated by the peptides, GUVs containing either peptide were mixed with N-NBD-PE-labeled GUVs and incubated in the presence of 2 mM $CaCl_2$ at RT or at 37°C in the absence of $CaCl_2$ for 2 h. Upon incubation, the GUVs were imaged as described above.

Results

Secondary structure of LV-peptides in liposomal membranes depends on primary structure

Figure 1 shows the LV-peptide sequences investigated here. The peptides are composed of a variable hydrophobic core that is flanked by Lys triplets, and a Trp residue is included for quantification. First, we investigated their secondary structures in liposomes, i.e., under conditions where their fusogenicities have previously been examined. Accordingly, peptides L16, LLV16, LV16, VVL16, and LV16-G8P9 were incorporated at a peptide/lipid (P/L) ratio of ~0.01 into liposomal membranes made by sonication of hydrated lipid/peptide mixtures (Hofmann et al. 2004). The membranes are composed of palmitoyl-oleoyl-phosphatidylcholine (POPC), di-oleoyl-phosphatidylethanolamine (DOPE), and

di-oleoyl-phosphatidylserine (DOPS) (3:1:1). These synthetic lipids exhibit substantially less background signal in spectroscopy than the natural lipid mixture used in previous fusion experiments (Hofmann et al. 2004). Yet, they support LV-peptide mediated liposome fusion as efficiently as the natural mixture (our unpublished results). Flotation of the liposomes in sucrose gradients confirmed that peptides were quantitatively associated with lipid since free peptides located at the bottom of the gradients were below detectable levels (results not shown). CD spectra were recorded from these liposomes, corrected for background spectra recorded with pure liposomes, and converted to molar ellipticities based on the experimentally determined peptide concentrations. The results shown in Fig. 2 a reveal that L16, LLV16, and LV16 give rise to spectra with double minima at 208 and 222 nm that are typical of α-helices. In contrast, the LV16-G8P9 spectrum is characterized by a single minimum at 218 nm that is diagnostic of *β*-sheet. The VVL16 spectrum has an intermediate line shape. The spectra were evaluated using an algorithm that is based on a set of peptide reference spectra (Poschner et al. 2007) in terms of percentage α-helix, *β*-sheet, turn, and random coil contents. L16, LLV16, and LV16 peptides display ∼70–80% of α-helical structure. In contrast, VVL16 is only ∼50% α-helical and helicity drops to ∼20% with LV16-G8P9. Non-helical secondary structure is mainly accounted for by *β*-sheet (Fig. 2b, Table 1). Turn and random coil structures account for only 3–12% of the secondary structure. Comparing the secondary structure contents to the previously determined fusogenicities (Fig. 2b) reveals that increasing fusogenicity is related to decreasing helix/sheet ratios. This is most pronounced with our most fusogenic variant, LV16-G8P9 that is characterized by predominantly *β*-sheet structure.

To examine whether peptide structure changes upon fusing the liposomes, liposomes containing L16, LLV16, LV16, or LV16-G8P9 were incubated for 3 h at 37°C where extensive liposome fusion is known to occur (Hofmann et al. 2004). Comparing secondary structures before and after fusion did not reveal significant changes (results not shown). Thus, the distribution of secondary structures appears to be stable.

L16	KKKWLLLLLLLLLLLLLLLLKKK
LLV16	KKKWLLVLLVLLVLLVLLVLKKK
LV16	KKKWLVLVLVLVLVLVLVLVKKK
VVL	KKKWVVLVVLVVLVVLVVLVKKK
V16	KKKWVVVVVVVVVVVVVVVVKKK
LV16-G8P9	KKKWLVLVLVLGPVLVLVLVKKK

Fig. 1 Sequences of LV-peptides. All hydrophobic core structures are flanked by Lys-triplets. A Trp residue is incorporated for quantification

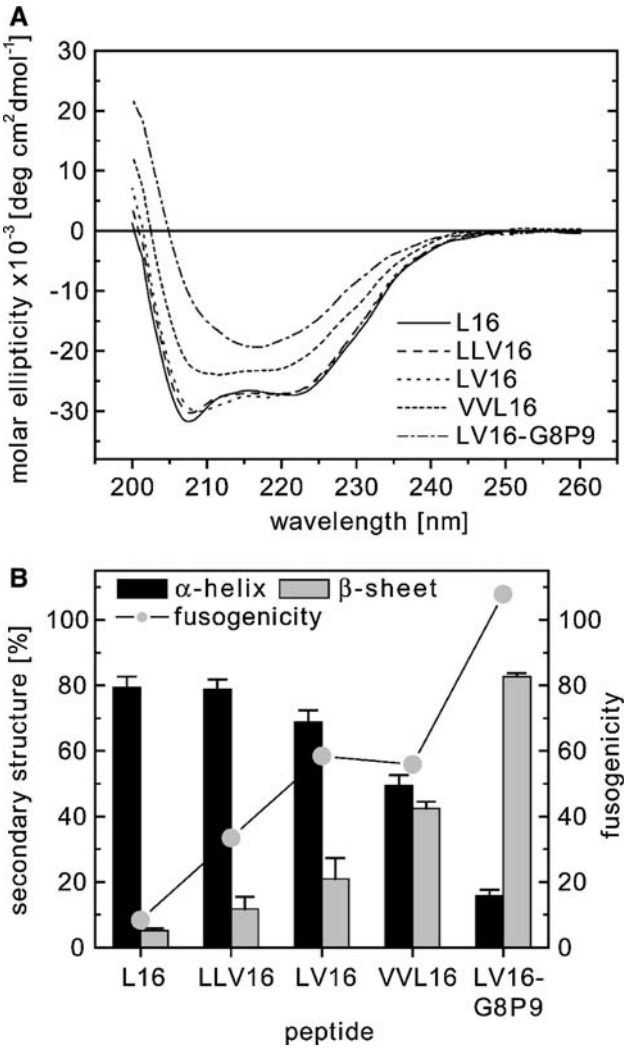

Fig. 2 Secondary structure of LV-peptides in liposomal membranes. **a** Representative CD spectra of liposomes made of POPC : DOPE : DOPS (3:1:1) containing L16, LLV16, LV16, VVL16, or LV16-G8P9 peptides at P/L ∼0.01. All spectra were corrected for the background signal generated by pure liposomes. **b** Secondary structure contents of the liposome-bound peptides as determined by deconvolution of CD spectral data. Only the contents in α-helix and *β*-sheet are given, turn and random coil structures collectively account for 3–12% of secondary structure. The values represent mean ± SD from four independent experiments. To compare secondary structures with the previously determined fusogenicities, we also plotted a dimensionless measure of fusogenicity. This measure is defined as the slope of the dependence of fusion extent after 1 h on the experimentally determined P/L-ratio and corrects for slightly different reconstitution efficiencies of our peptides (Hofmann et al. 2004)

Alternative to peptide integration during liposome formation, the secondary structures of some peptides (L16, LV16, and LV16-G8P9) were determined after adding them from solutions in acetonitrile to preformed liposomes [final acetonitrile concentration <1% (v/v)]. Separating liposomes with bound peptides from unbound peptides by sucrose gradient centrifugation confirmed that the added

Table 1 Secondary structures of membrane-embedded peptides

Peptide	Liposomes[a]		Planar bilayers[b]							
	α-Helix	β-Sheet	α-Helix	R^c	Θ_α^d	β-Sheet			Turn	Random coil
						Total	Parallel	Antiparallel		
L16	79	5	69	1.52	37°	22	14	8	5	4
LLV16	79	12	30	1.64	33°	13	11	2	34	23
LV16	69	21	29	1.60	34°	56	51	5	7	8
VVL16	49	42	22	2.07	22°	50	49	1	11	16
V16	n.d.[d]	n.d.	5	4.01	n.d.[e]	73	41	32	10	11
LV16-G8P9	16	83	7	1.49	38°	54	26	28	21	17

[a] Secondary structure contents in liposomal membranes were determined by CD spectroscopy. Contents in turn and random coil are not given here since they accounted for <12% of total secondary structures

[b] Secondary structure contents in planar bilayers as determined by FTIR spectroscopy

[c] Dichroitic ratio of α-helix assigned bands

[c] Θ Denotes the average tilt angle of the α-helix relative to the bilayer normal

[e] *n.d* not determined

peptides were quantitatively associated with the liposomes. While L16 is still largely (~80%) α-helical under these conditions, LV16 folds into ~25% α-helix, ~35% β-sheet, ~23% random coil, and ~17% β-turn. LV16-G8P9 exhibited approximately equal amounts of β-sheet and random coil (~45%, each) plus very small contents of α-helix and β-turn. The discrepancy between these results (data not shown) and those obtained with the co-reconstitution method suggest that helix and sheet structures displayed by the membrane-bound LV16 and LV16-G8P9 peptides are not at equilibrium. Rather, it appears that addition from solution results in a larger proportion of β-sheet than co-reconstitution, especially with the more flexible sequences.

We conclude that increased fusogenicity is compatible with a predominantly α-helical state up to LV16 while a further increase of the Val content or introduction of a Gly/Pro pair tips the balance toward β-sheet formation.

LV-peptides distribute homogenously and fuse giant unilamellar liposomes

Here, we first studied the lateral distribution of peptides in the membrane. To this end, rhodamine-tagged peptides Rh-LLV16 (low fusogenicity) or Rh-LV16-G8P9 (high fusogenicity) were incorporated at a P/L-ratio of ~0.01 together with the lipidic fluorophore C6-NBD-PC into giant unilamellar vesicles (GUVs) and visualized by fluorescence microscopy. A homogenous lateral distribution is found for Rh-LLV16 (Fig. 3a) and for Rh-LV16-GP (not shown) although both peptides exhibit vastly different secondary structures (see: Fig. 2). The distribution of the lipidic fluorophore C6-NBD-PC was examined for control (Fig. 3a). The homogenous distributions of both, peptides and lipid, indicate the absence of lipid microdomains in the GUV membranes at the scale of the observation.

To investigate potential GUV-GUV fusion, GUVs with rhodamine-tagged peptides were mixed with N-NBD-PE-labeled GUVs and incubated at room temperature. Figure 3 shows a galery of GUVs that exhibit colocalization of N-NBD-PE and Rh-LLV16 (Fig. 3b) or Rh-LV16-GP (Fig. 3c). The co-staining of GUVs by peptides and N-NBD-PE indicate their previous fusion. In the absence of peptides, fusion between N-Rh-PE GUVs and N-NBD-PE GUVs was only rarely observed.

The α-helices of aliphatic LV-peptides span planar bilayers at oblique angles

Secondary structures and transmembrane orientation of LV-peptides were also examined in planar bilayers composed of the same lipids as the liposomes. To this end, we analyzed stacked oriented hydrated bilayers containing the peptides at P/L ~0.01 on the surface of an internal reflection element (IRE) with ATR-FTIR spectroscopy. The following results were obtained by decomposition of the conformation-sensitive amide I extinction band between 1,700 and 1,600 cm^{-1} (Fig. 4, Table 1): The L16 amide I band is dominated by a component at 1,656 cm^{-1} that is diagnostic for α-helical structure. Deconvolution of the spectral envelope revealed that the helix accounts for 69% of total secondary structure. The remaining structure corresponds to parallel and antiparallel β-sheet, β-turn, and random coil. The LLV16 spectrum indicated only 30%

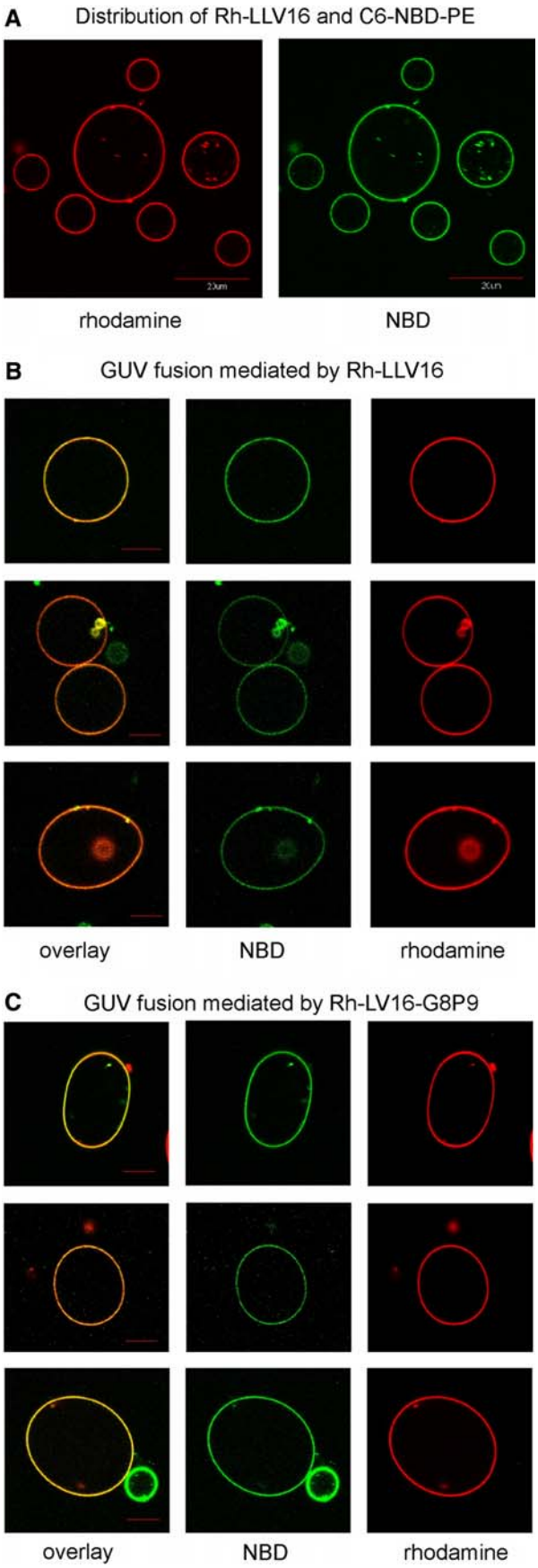

◀ **Fig. 3** Distribution and fusogenic activity of LV-peptides in membranes of Giant Unilamellar Vesicles. **a** GUVs (POPC : DOPE : DOPS at a 3:1:1 ratio) containing Rh-LLV16 at P/L ~0.01 (visualized by detecting rhodamine fluorescence in the *left panel*) and 1 mol% C6-NBD-PC (visualized by detecting NBD fluorescence in the *right panel*) show a homogeneous distribution of peptide and C6-NBD-PC. **b, c** GUVs containing either Rh-LLV16 (**b**) or Rh-LV16-G8P9 (**c**) at P/L = 0.01 were incubated with N-NBD-PE (1 mol%) labeled GUVs (see main text). Detection of GUVs that exhibit both rhodamine and NBD fluorescence indicates successful fusion. *Bar* = 10 μm

α-helix, while turn and random coil structures were more prevalent. LV16 and VVL16 gave 29 and 22% α-helix, respectively. Now, parallel β-sheet conformation, as reflected by the band at 1,630 cm^{-1}, becomes the dominating structural element. LV16-G8P9 behaves very differently. Here, the α-helical component is of very low intensity (7%); at the same time, antiparallel and parallel β-sheet structures were equally abundant. We also investigated an oligo-Val (V16) peptide. This sequence forms mainly β-sheet (73%) where parallel strand orientation is slightly more prevalent than the antiparallel one (spectrum not shown). Figure 4 F represents a bar diagram for easy comparison of the results.

The orientation of the α-helices in the membrane was determined by exploitation of their dichroitic effects as measured with polarized IR light. After decomposition of amide I bands measured with infrared light that was polarized in parallel or perpendicular to the IRE plane, dichroitic ratios of the components assigned to α-helices were used to calculate the mean helix angle relative to the membrane normal. The results revealed that most helices adopted oblique angles ranging from 34° to 38° relative to the bilayer normal (Fig. 5, Table 1). The VVL16 helix appeared to be less tilted (22°) for reasons that are not clear. The minor helical fraction of V16 did not exhibit sufficient absorption to allow determination of the insertion angle. In control experiments with bR in native purple membranes (Fig. 5), our experimental approach yielded an average tilt angle of 15° of the TMDs relative to the membrane normal which is close to their mean angle derived from X-ray crystallography (12.4°) (PDB code 1QHJ). The Schiff base of bR was used as reference plane for the membrane in the crystal structure. Unfortunately, data quality was insufficient to satisfactorily analyze the orientation of the β-strand fractions of the peptides. The extinction of the peptides in the few stacked bilayers was too weak in the amide II region to interpret dichroitic effects according to ref (Marsh 1997).

We conclude that (a) increasing the Val content of the core strongly decreases the helix/sheet ratio of the peptides in planar bilayers and that (b) the α-helical populations traverse the lipid bilayer at oblique angles.

Discussion

The main objective of the present study was to reveal the secondary structure of LV-peptides in membranes. In small unilamellar vesicular (SUV) membranes, i.e., under conditions of the standard fusion assay, we find that successively increasing the Val/Leu ratio of the peptides largely maintains α-helicity of L16, LLV16, and LV16 peptides. In contrast, VVL16 and LV16-G8P9 exhibit strongly decreased helix/sheet ratios. In oriented planar bilayers, a more pronounced decrease in the helix/sheet ratio is seen upon introducing Val. Again, a further drop in helicity is seen with LV16-G8P9 which is largely compensated for by increased turn formation. The secondary structure of V16 is dominated by β-sheet. V16 cannot be analyzed in liposomes due to its very low reconstitution efficiency (Hofmann et al. 2004). Although there is a similar trend in the dependence of secondary structure preference on the core sequence in both membrane systems, LLV16, LV16, and VVL16, i.e., those peptides with intermediate fusogenicities, exhibit lower helix/sheet ratios in planar bilayers compared to liposomes. On the other hand, L16 and LV16-G8P9 behave similarly in liposomes and bilayers. These peptides exhibit the lowest and highest fusogenicities, respectively. It thus appears that the secondary structures of peptides of very low (L16) or very high (LV16-G8P9) fusogenicity are rather independent of the type of membrane system while peptides with intermediate fusogenicity (LLV16, LV16, and VVL16) may express conformational preferences that may depend on the method of sample preparation, on membrane curvature, and/or on the degree of membrane hydration.

One may argue that the ability of our LV-peptides to fuse sonicated SUVs depends on the high curvature stress of these membranes. Our present results, however, show that two exemplary rhodamine-tagged variants are capable of driving GUV-GUV fusion, too. Although the efficiency of peptide-driven GUV-GUV fusion is difficult to compare quantitatively to the efficiency of SUV-SUV fusion, this

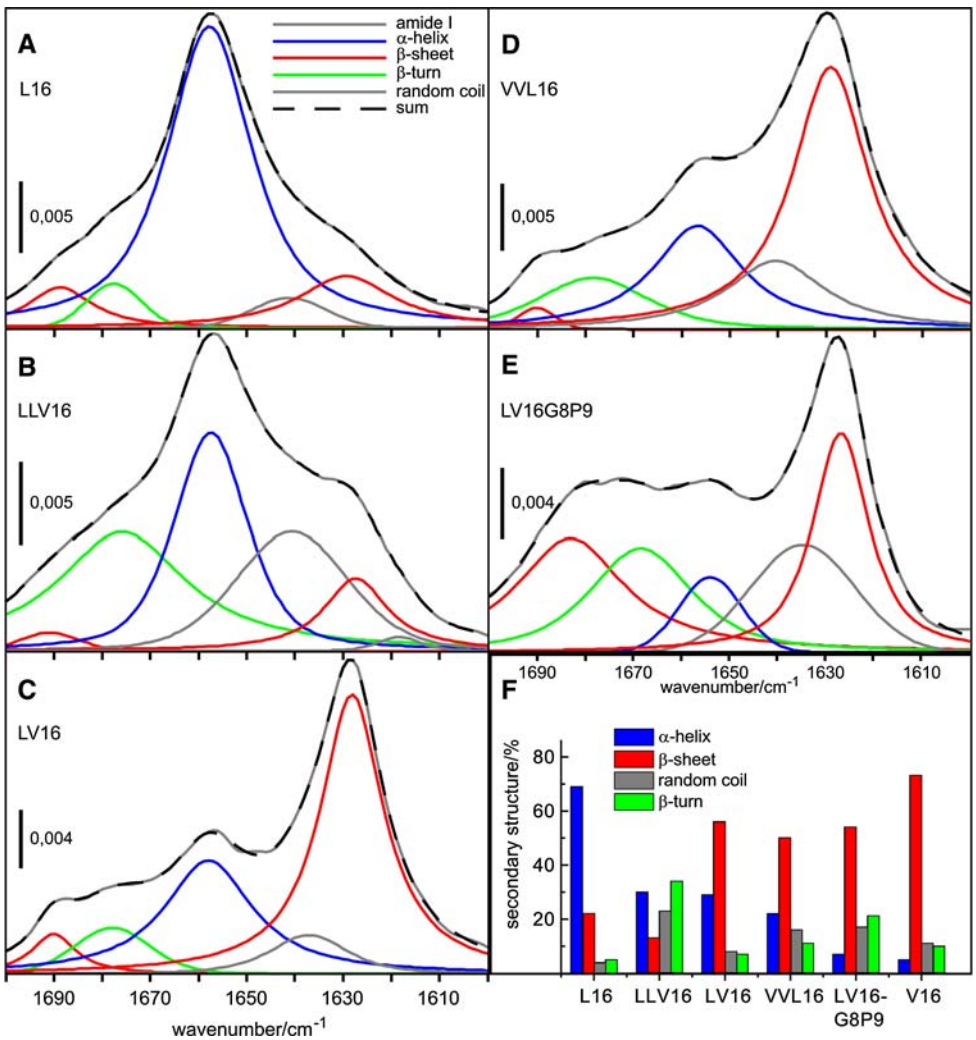

Fig. 4 Secondary structure of LV-peptides in planar membranes **a–e**. FTIR-spectra of LV-peptides in thin hydrated membrane stacks of POPC : DOPE : DOPS (3:1:1). Amide I band decomposition reveals that L16 (**a**) is mainly α-helical while LLV16 (**b**) has significant contents of β-turn and random coil. LV16 (**c**) and VVL16 (**d**) are characterized by a dominating parallel β-sheet component while the band shape of LV16-G8P9 (**e**) indicates an additional high-frequency component assigned to antiparallel β-sheet. The spectral envelopes are represented by continuous *gray lines* while the respective sum of fitted components corresponds to the broken lines. **f** Graphic representation of secondary structure fractions as given in Table 1. β-Sheet contents represent the sum of parallel and antiparallel sheet

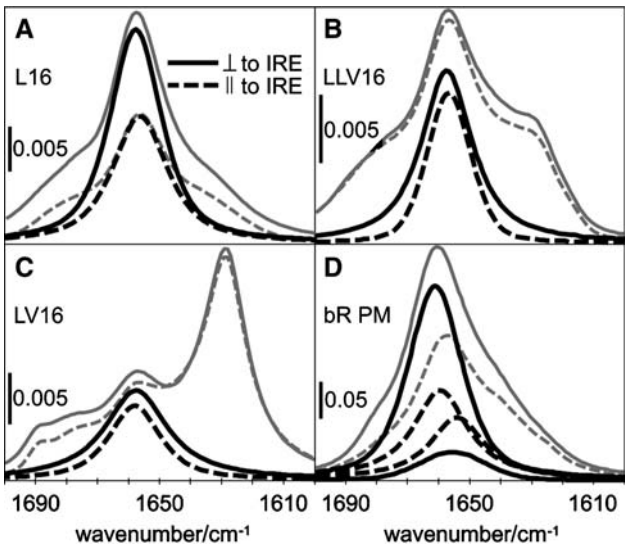

Fig. 5 Orientation of membrane-embedded peptides. Polarized amide I band envelopes (*thin gray lines*) and their components assigned to α-helix (*bold black lines*) indicate non-isotropic helix orientation. **a–c** Peptide helix tilt angles toward the membrane normal (**a**: L16, 37°; **b**: LLV16, 33°; **c**: LV16, 34°) were calculated from dichroitic ratios of the integrated component areas. **d** Control experiment showing that the α-helices of bacteriorhodopsin in purple membranes (bR PM) adopt an average tilt angle of 15° relative to the membrane normal. Two helix-assigned components were necessary for reliable band decomposition of the bacteriorhodopsin amide I band. The dichroitic ratio was calculated as relation of the summed integrals of both components

demonstrates the principal ability of LV-peptides to facilitate complete mixing of low-curvature bilayers.

In principle, the spectroscopic data obtained with the different membrane systems are consistent with the existence of peptides that are partially α-helical and partially β-sheet/disordered as recently shown for the hydrophobic fusion domain of human immunodeficiency virus in micelles (Li and Tamm 2007). Unlike this natural sequence, our LV-peptides have symmetric sequences and are thus unlikely to insert into the bilayer in a partially helical conformation. We therefore favor the idea that LV-peptides form distinct populations that fold into the different conformations determined experimentally.

A deliberate effort to distinguish between parallel and anti-parallel β-sheets by FTIR spectroscopy suggests that the β-strands of LV16-G8P9 assume equally frequent parallel and anti-parallel orientations. Although the bands signifying antiparallel sheet and turn overlap, this peptide also appears to exhibit a large fraction of turn structure. This suggests that the peptide backbone forms a turn at the central Gly/Pro pair and folds back upon itself. This hairpin structure may self-assemble to larger aggregates at a submicroscopic level via intermolecular parallel chain-chain interactions. V16, the only other peptide with significant anti-parallel β-sheet structure has a much lower apparent turn content and thus may predominantly self-associate by way of straight β-strands.

The rank order of peptides in terms of increasing sheet/helix ratio roughly reflects the rank order of fusogenicity determined previously (Hofmann et al. 2004). How is the sheet/helix ratio mechanistically related to fusogenicity? In principle, bilayer mixing could be elicited by the α-helix, the β-sheet, or by dynamically interconverting secondary structures. For the following reasons we consider dynamic interconversion as unlikely. First, transition from α-helix to β-sheet and vice versa is likely to require transient unfolding and thus exposure of peptide backbone carbonyl and amide groups. As exposure of the hydrogen–bond donors and acceptors within the apolar bilayer is energetically unfavorable, helix/sheet transitions are unlikely to occur in membranes unless the transition proceeds without an unfolded intermediate structure. Second, if membrane-bound helix and sheet structures were dynamically interconverting, addition of peptides to preformed liposomes should result in the same helix/sheet ratio as with co-reconstitution. At least with both fusogenic peptides tested (LV16 and LV16-G8P9) this was clearly not the case as addition of these peptides to liposomes resulted in significantly less helix and more sheet and random coil structures than co-reconstitution with lipids. We thus propose that the different secondary structures are kinetically stable in the membrane. Further, the helix/sheet ratios do not change upon prolonged incubation or fusion of liposomes. Thus, these ratios are thought to reflect the probability by which a given peptide folds into α-helix or β-sheet at the time of membrane formation.

If fusion is not induced by rapidly interconverting helices and sheets, the question is whether the fusogenic conformation corresponds to α-helix or to β-sheet. At present, we cannot answer this question with certainty. Since L16, LLV16, and LV16 are mainly α-helical in liposomal membranes we consider it likely that a membrane-spanning α-helix represent the fusogenic conformation of an LV-peptide with an aliphatic core. Fusogenicity of the helix may require a flexible backbone that fluctuates around its idealized conformation in the lipid membrane. The frequency of these hypothesized fluctuations, and by implication the extent of fusogenicity, may depend on the content in Val whose β-branched side-chain disfavors the helical conformation (Chellgren and Creamer 2006). This proposition is in line with the recent finding that the conformationally flexible human immunodeficiency virus gp41 fusion peptide gp41 induces lipid mixing at concentrations that support the α-helical, but not the β-strand, conformation (Li and Tamm 2007).

Previously, the fusogenicity of various membrane-associated α-helical peptides has been related to their ability to adopt oblique angles within the bilayer which is

thought to disrupt lipid packing (Brasseur 2000). In case of our model peptides, however, tilt angles and fusogenicity are not correlated and an oblique orientation per se is thus unlikely to elicit membrane fusion.

A fusogenic α-helical conformation of aliphatic LV-peptides (LLV16 to VVL16) is consistent with the α-helicity of natural fusion protein TMDs (Bowen and Brunger 2006; Xu et al. 2005; Zhang and Shin 2006). One interesting result of the present study is that the Val content (50%) of the LV16 core, that is still mainly α-helical in liposomal membranes, matches the combined content of Val plus Ile (~50%) of SNARE TMDs (Langosch et al. 2001b). On the other hand, unrelated TMDs contain only ~25% of both β-branched amino acids (Arkin and Brünger 1998). One may speculate, therefore, that 50% is close to the maximal content of β-branched amino acids that allows for formation of a membrane-spanning α-helix.

Conformational flexibility may also be relevant for the function of natural fusion protein TMDs. For example, the TMD of influenza hemagglutinin showed relatively rapid amide hydrogen exchange. Although the exchange kinetics were tentatively attributed to pore formation by this TMD (Tatulian and Tamm 2000) this observation is equally consistent with significant structural dynamics of the helix. In case of the yeast SNARE Sso1p, electron paramagnetic resonance spectra indicated increased dynamics of the C-terminal half of the α-helical TMD (Zhang and Shin 2006). One may therefore speculate that restricted conformational flexibility is shared by LV-peptides and the TMDs of natural fusogenic proteins.

Insertion of a Gly/Pro pair into the LV-helix, like in LV16-G8P9, further increases fusogenicity. In this case, however, β-sheet, turn, and random coil account for the major secondary structures with only little α-helix remaining. The turn may separate short β-strand and/or α-helical domains resulting in an hairpin structure. Lipid mixing induced by LV16-P8G9 may thus be related to β-sheet formation as proposed for a number of flexible fusogenic amphipathic peptides of natural origin (Nieva et al. 1994; Yang et al. 2004) (Muga et al. 1994) (Dupiereux et al. 2005).

Acknowledgments This work was supported by a grant from the Volkswagen Foundation as part of the project "Conformational Control of Biomolecular Function" to D. L. and K. G.

References

Angelova M, Soléau S, Méléard P, Faucon JF, Bothorel P (1992) Preparation of giant vesicles by external AC electric fields: kinetics and application. Prog Colloid Polym Sci 89:127–131

Arkin IT, Brünger AT (1998) Statistical analysis of predicted transmembrane alpha-helices. Biochim Biophys Acta 1429:113–128

Armstrong RT, Kushnir AS, White JM (2000) The transmembrane domain of influenza hemagglutinin exhibits a stringent length requirement to support the hemifusion to fusion transition. J Cell Biol 151:425–437

Arrondo JL, Muga A, Castresana J, Goñi FM (1993) Quantitative studies of the structure of proteins in solution by Fourier-transform infrared spectroscopy. Prog Biophys Mol Biol 59:23–56

Bandekar J (1992) Amide modes and protein conformation. Biochim Biophys Acta 1120:123–143

Bechinger B, Ruysschaert JM, Goormaghtigh E (1999) Membrane helix orientation from linear dichroism of infrared attenuated total reflection spectra. Biophys J 76:552–563

Bowen M, Brunger AT (2006) Conformation of the synaptobrevin transmembrane domain. Proc Natl Acad Sci 103:8378–8383

Brasseur R (2000) Tilted peptides: a motif for membrane destabilization (hypothesis). Mol Membr Biol 17:31–40

Byler DM, Susi H (1986) Examination of the secondary structure of proteins by deconvolved FTIR spectra. Biopolymers 25:469–487

Chellgren BW, Creamer TP (2006) Side-chain entropy effects on protein secondary structure formation. PROTEINS: Struct Funct Bioinform 62:411–420

Cleverley DZ, Lenard J (1998) The transmembrane domain in viral fusion: essential role for a conserved glycine residue in vesicular stomatitis virus G protein. Proc Natl Acad Sci USA 95:3425–3430

Dennison SM, Greenfield N, Lenard J, Lentz BR (2002) VSV transmembrane domain (TMD) peptide promotes PEG-mediated fusion of liposomes in a conformationally sensitive fashion. Biochemistry 41:14925–14934

Dupiereux I, Zorzi W, Lins L, Brasseur R, Colson P, Heinen E, Elmoualij B (2005) Interaction of the 106–126 prion peptide with lipid membranes and potential implication for neurotoxicity. Biochem Biophys Res Commun 331:894–901

Giraudo CG, Hu C, You DQ, Slovic AM, Mosharov EV, Sulzer D, Melia TJ, Rothman JE (2005) SNAREs can promote complete fusion and hemifusion as alternative outcomes. J Cell Biol 170:249–260

Goormaghtigh E, Cabiaux V, Ruysschaert JM (1994) Determination of soluble and membrane protein structure by Fourier transform infrared spectroscopy. III. Secondary structures. Subcell Biochem 23:405–450

Goormaghtigh E, Ruyschaert JM (1990) Polarized attenuated total reflection infrared spectroscopy as a tool to investigate the conformation and orientation of membrane components. In: Brasseur R (ed) Molecular description of biological membrane components by computer-aided conformational analysis, vol I. CRC Press, Boca Raton, pp 285–328

Goormaghtigh E, Ruysschaert J-M (1994) Subtraction of atmospheric water contribution in Fourier transform infrared spectroscopy of biological membranes and proteins. Spectrochim Acta 50A:2137–2144

Harrick NJ (1967) Internal reflection spectroscopy. Interscience Publishers, Wiley, New York

Hofmann MW, Peplowska K, Rohde J, Poschner B, Ungermann C, Langosch D (2006) Self-interaction of a SNARE transmembrane domain promotes the hemifusion-to-fusion transition in lipid mixing. J Mol Biol 364:1048–1060

Hofmann MW, Weise K, Ollesch J, Agrawal A, Stalz H, Stelzer W, Hulsbergen F, deGroot H, Gerwert K, Reed J, Langosch D (2004) De novo design of conformationally flexible transmembrane peptides driving membrane fusion. Proc Natl Acad Sci USA 101:14776–14781

Jahn R, Scheller RH (2006) SNAREs—engines for membrane fusion. Nat Rev Mol Cell Biol 7:631–643

Kemble GW, Danieli T, White JM (1994) Lipid-anchored influenza hemagglutinin promotes hemifusion, not complete fusion. Cell 76:383–391

Krimm S, Bandekar J (1986) Vibrational spectroscopy and conformation of peptides, polypeptides, and proteins. Adv Protein Chem 38:181–364

Langosch D, Brosig B, Pipkorn R (2001a) Peptide mimics of the vesicular Stomatitis virus G-protein transmembrane segment drive membrane fusion in vitro. J Biol Chem 276:32016–32021

Langosch D, Crane JM, Brosig B, Hellwig A, Tamm LK, Reed J (2001b) Peptide mimics of SNARE transmembrane segments drive membrane fusion depending on their conformational plasticity. J Mol Biol 311:709–721

Langosch D, Hofmann MW, Ungermann C (2007) The role of transmembrane domains in membrane fusion. Cell Mol Life Sci 64:850–864

Li Y, Tamm LK (2007) Structure and plasticity of the human immunodeficiency virus gp41 fusion domain in lipid micelles and bilayers. Biophys J 93:876–885

Marsh D (1997) Dichroic ratios in polarized Fourier transform infrared for nonaxial symmetry of beta-sheet structures. Biophys J 72:2710–2718

Melikyan GB, Lin SS, Roth MG, Cohen FS (1999) Amino acid sequence requirements of the transmembrane and cytoplasmic domains of influenza virus hemagglutinin for viable membrane fusion. Mol Biol Cell 6:1821–1836

Muga A, Neugebauer W, Hirama T, Surewicz WK (1994) Membrane interaction and conformational properties of the putative fusion peptide of PH-30, a protein active in sperm-egg fusion. Biochemistry 33:4444–4448

Nieva JL, Nir S, Muga A, Goni FM, Wilschut J (1994) Interaction of the HIV-1 fusion peptide with phospholipid vesicles: different structural requirements for fusion and leakage. Biochemistry 33:3201–3209

Nüssler F, Clague MJ, Herrmann A (1997) Meta-stability of the hemifusion intermediate induced by glycosylphosphatidylinositol-anchored influenza hemagglutinin. Biophys J 73:2280–2291

Ollesch J, Künnemann E, Glockshuber R, Gerwert K (2007) Prion protein alpha-to-beta transition monitored by time-resolved Fourier transform infrared spectroscopy. Appl Spectrosc 61:1025–1031

Poschner B, Reed J, Langosch D, Hofmann MW (2007) An automated application for deconvolution of circular Dichroism spectra of small peptides. Anal Biochem 363:306–308

Rothschild KJ, Clark NA (1979) Polarized infrared spectroscopy of oriented purple membrane. Biophys J 25:473–487

Roy R, Peplowska K, Rohde J, Ungermann C, Langosch D (2006) Role of the Vam3p Transmembrane segment in Homodimerization and SNARE complex formation. Biochemistry 45:7654–7660

Seul M, Sammon MJ (1990) Preparation of surfactant multilayer films on solid substrates by deposition from organic solution. Thin Solid Films 185:287–305

Surewicz WK, Mantsch HH (1990) The conformation of proteins and peptides in a membrane environment: an infrared spectroscopic approach. Biotechnology 14:131–157

Surewicz WK, Mantsch HH, Chapman D (1993) Determination of protein secondary structure by Fourier transform infrared spectroscopy: a critical assessment. Biochemistry 32:389–394

Tamm LK, Crane J, Kiessling V (2003) Membrane fusion: a structural perspective on the interplay of lipids and proteins. Curr Opin Struct Biol 13:453–466

Tatulian SA (2003) Attenuated total reflection Fourier transform infrared spectroscopy: a method of choice for studying membrane proteins and lipids. Biochemistry 42:11898–11907

Tatulian SA, Tamm LK (2000) Secondary structure, orientation, oligomerization, and lipid interactions of the transmembrane domain of influenza hemagglutinin. Biochemistry 39:496–507

Xu Y, Zhang F, Su Z, McNew JA, Shin Y-K (2005) Hemifusion in SNARE-mediated membrane fusion. Nat Struct Mol Biol 12:417–422

Yang J, Prorok M, Castellino FJ, Weliky DP (2004) Oligomeric beta-structure of the membrane-bound HIV-1 fusion peptide formed from soluble monomers. Biophys J 87:1951–1963

Zhang Y, Shin Y-K (2006) Transmembrane organization of yeast syntaxin-analogue Sso1p. Biochemistry 45:4173–4181

Zhang YP, Lewis RN, Henry GD, Sykes BD, Hodges RS, McElhaney RN (1995) Peptide models of helical hydrophobic transmembrane segments of membrane proteins. 1. Studies of the conformation, intrabilayer orientation, and amide hydrogen exchangeability of Ac-K2-(LA)12-K2-amide. Biochemistry 34:2348–2361